Preface

Derived from the Greek word tribos, meaning friction, the word tribology was first used in 1966 in Great Britain to describe the scientific and technical domains focused on the study of friction, wear and lubrication.

Tribology addresses such questions as: what is the best way to reduce wear and control friction? What materials should be used? What lubricant should be chosen to protect a motor or manufacture a particular component? What surface treatment should be applied to improve the wear resistance and reliability of a mechanical system?

Despite their apparent simplicity, the problems of tribology are in fact very complex. They involve the bulk properties of materials as well as their microscopic surface characteristics and their interaction with the surrounding environment.

By providing solutions in fields as diverse as car manufacturing and medical prosthesis, tribology can have a significant economic and ecological impact. For instance, if we can reduce friction in a motor, we reduce energy consumption and limit pollution. If we can reduce the wear in a cutting tool, we both increase productivity and improve the quality of manufactured products. If we can limit ball bearing and gearbox wear, then we can increase the life-span and improve the reliability of many different mechanical systems. If we can reduce friction in an artificial hip, then we can avoid production of wear-particles that can induce inflammation and cause serious complications such as osteolysis or even loosening of the joint itself.

Because tribological phenomena are by nature complex, solving them requires a multidisciplinary approach combining techniques derived from mechanics, solid-state physics and surface chemistry. This sometimes makes it seem like a poorly defined subject, and raises a number of challenges for effective teaching. The

purpose of this book is therefore to make tribology comprehensively accessible, by illustrating its principles and its applications through a variety of case studies taken from the scientific as well as the industrial domains. In both its content and structure, *Materials and Surface Engineering in Tribology* is designed to provide a clear, synthetic overview of the field, and therefore serve as a reference book suitable for students, researchers and engineers alike.

Materials and Surface Engineering in Tribology is divided into three chapters:

Chapter 1 introduces the notion of a surface in tribology where a solid surface is described from the topographical, structural, mechanical and energetic points of view. It also describes the principal techniques used to characterize and analyze surfaces.

Chapter 2 discusses what may be called tribology proper by introducing and describing the concepts of adhesion, friction, wear and lubrication.

Chapter 3 focuses on the materials used in tribology. We introduce the major classes of materials used, either in their bulk states or as coatings, including both hard-facing protective layers and other coatings used for decorative purposes.

2.5.2. *Surface forces measurements*

Surface forces are primarily studied with two kinds of devices: the *surface forces apparatus* (SFA) or the *atomic force microscope* (AFM).

2.5.2.1. *The surface forces apparatus (SFA)*

The principle of the SFA is to carefully bring together a mobile surface (a plane or sphere) and a fixed surface (a plane) and to measure, during approach and withdrawal, their forces of interaction as well as the distance between them [GEO 94].

Figure 2.26 shows the evolution of the force depending on the phase of approach or withdrawal for two carbon surfaces, a sphere and a plane, in a dry atmosphere. During approach, a jump to contact resulting from Van der Waals forces occurred. During withdrawal, some hysteresis is noted and the maximum adhesive force (436 mN m^{-1}) can easily be deduced. Based on this quantity, the surface energy of carbon can be calculated by applying the JKR model (see Table 2.1) and equation [2.21]:

$$\gamma = \frac{F_{ad}}{3\pi R} \qquad [2.36]$$

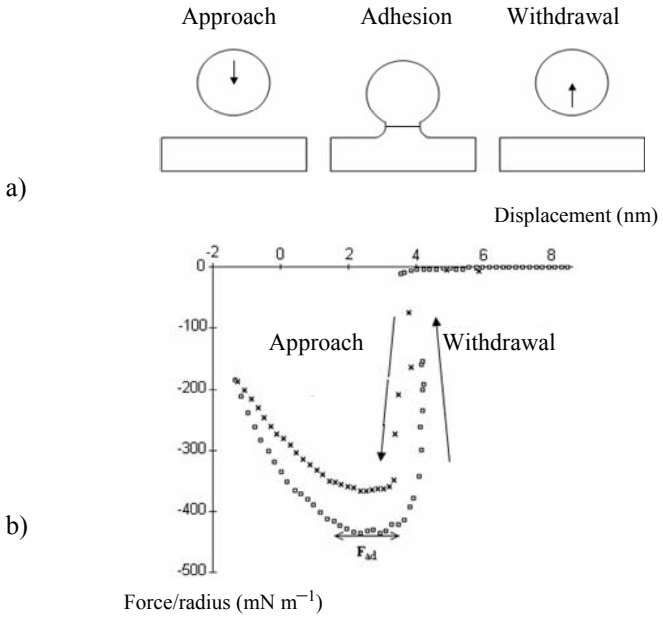

Figure 2.26. *Forces of adhesion of a sphere on a plane. Forces curve obtained for two carbon surfaces with an SFA used in dry air: a) displacement of the sphere; b) force curves [GEO 00]*

Figure 2.27 shows the impact of humidity on the force profile for two carbon surfaces. The curves shown are for the withdrawal phase. We see clearly that the maximum adhesive force (476 mN m^{-1}) measured in a wet atmosphere (relative humidity 30%) is greater than the equivalent for measurements in a dry atmosphere. Moreover, the shape of the curve clearly provides evidence for the generation of an interfacial meniscus (the withdrawal phase is accompanied by a strong tail on the curve).

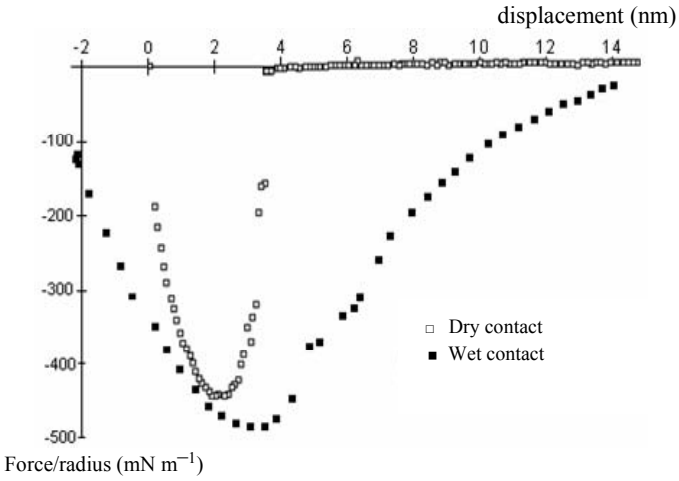

Figure 2.27. *Force profile relative to displacement during withdrawal of the sphere from the carbon plane; curves recorded in dry and wet conditions [GEO 00]*

2.5.2.2. *The atomic force microscope (AFM)*

The principle of the AFM was presented in section 1.2.2.3.3. This technique offers better resolution both in terms of the applied force as well as vertical displacement, and also allows improved spatial resolution as the radius of curvature of the AFM tip ranges from a few nanometers to a few tens of nanometers (whereas spheres used in SFAs have radii of several millimeters).

We now present some measurement results obtained from experiments carried out on immersed surfaces in different electrolytes.

Two metallic surfaces dipped in an electrolyte are brought close together. Depending on the nature of the environment, the materials, the adsorbed species and the pH of the solution, the surfaces may be subject to attraction or repulsion under the action of a range of forces such as hydrophobia, hydration,Van der Waals forces or electrostatic forces [BHU 05].

Consider using an AFM to study the particular case of the contact between different materials in a solution with differences in pH. We know that for a given electrolyte, the material's surface will develop a negative charge beyond a certain threshold pH (pH_S) and will develop a positive charge below this threshold. The point corresponding to a surface charge of zero ($pH = pH_S$) is known as the isoelectric point or IEP.

As the tip of the AFM is made of silicon nitride (Si_3N_4) (whose IEP corresponds to a pH of 6), then depending on the nature of the material (i.e. its IEP) brought into contact with the tip in a given electrolyte, the two surfaces will develop same-sign or opposite sign charges and repulse or attract.

Figure 2.28a shows force curves corresponding to the contact between the tip of the AFM (Si_3N_4) and a silicon oxide sample, in a 1 mM NaCl electrolyte solution, at pH 4 and at pH 8.5. Silicon oxide has an IEP of pH 2, so its interaction with silicon nitride (of IEP pH 6) will be attractive between pH 2 and pH 6 (the case for pH 4) and repulsive otherwise (the case for pH 8.5) [MARTI 95]. For the pH 4 case, we note that there is a large degree of hysteresis corresponding to strong adhesion between the surfaces. However, at pH 8.5 the force curve shows repulsion between the surfaces.

Figure 2.28b shows force curves for a polycrystalline nickel sample in contact with the tip of the AFM (Si_3N_4) in a 1 mM NaCl electrolyte solution at pH 3.3 and at pH 10.5. Nickel is negatively charged irrespective of pH whereas silicon nitride (IEP pH 6) is positively charged at pH 3.3 (attraction between Ni and Si_3N_4), and negatively charged at pH 10.5 (repulsion between Ni and Si_3N_4). The attraction, which is associated with a strong adhesive force, is clearly illustrated by the hysteresis in the adhesion measured at pH 3.3 [GAV 02a].

As a result of experiments in nanotribology, a new approach to the interpretation of friction has been introduced by Israelachvili [ISR 94]. He has shown that friction is not correlated to the force of adhesion (strength of formed junctions), but to adhesion hysteresis, i.e. the energy expended during the adhesion–rupture cycle.

This energy represents the difference between the energy required to establish and break the contact. It reflects the irreversibility of the force responsible for the adhesion, whereas in the Tabor and Bowden model, it is the value of this force that determines the degree of friction.

Figure 2.29 enables the unambiguous verification of this model. These results are from the system described above and are shown in Figure 2.28a. Several force curves were recorded at different pH levels and friction forces were measured with a lateral force microscope (LFM) (see section 1.2.2.3.3). We note perfect correlation between the adhesion hysteresis and the friction force.

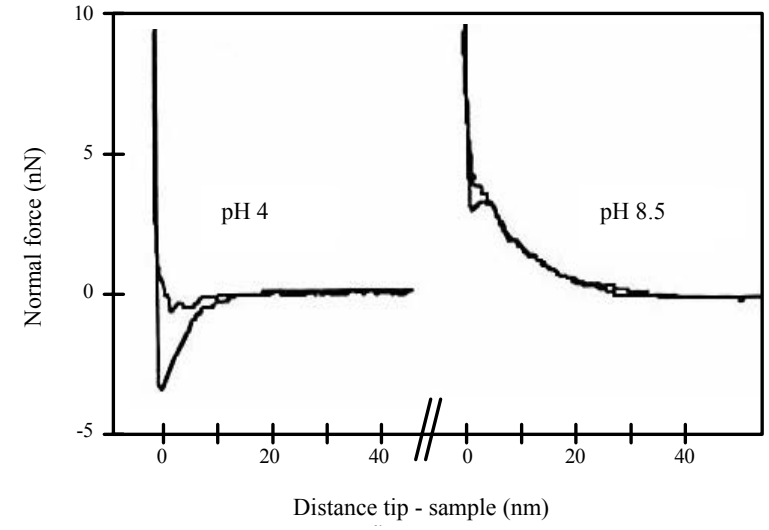

a)

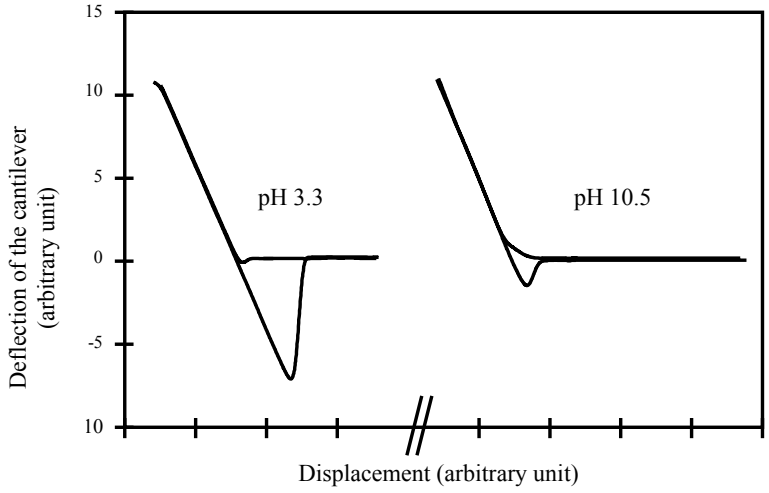

b)

Figure 2.28. *a) Force curve recorded at pH 4 and pH 8.5 in a solution of 1 mM of NaCl between the silicon nitride tip of the AFM and a silicon oxide sample [MARTI 95]; b) force curve recorded at pH 3.3 and pH 10.5 in a solution of 1 mM of NaCl between the silicon nitride tip of the AFM and a nickel sample [GAV 02a] (see Figure 1.18 for the interpretation of force curves)*

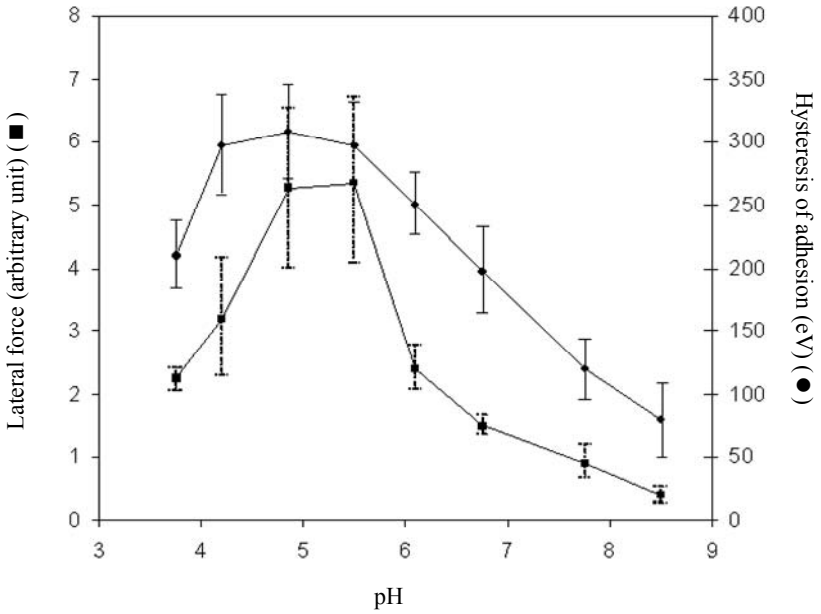

Figure 2.29. *Lateral force (friction force) (■) and expended energy (hysteresis of adhesion) (●) measured with AFM/LFM at different levels of pH in a solution of 1 mM of NaCl between the silicon nitride tip of the AFM and a silicon oxide sample [MARTI 95]*

2.5.2.3. *Application: surface forces and micromanipulation*

As shown in Table 2.3, as the dimensions of an object reduce, there is an increase in the surface area to volume ratio, which results in surface forces playing an increasingly important role in interactions. This is perfectly illustrated in the field of micromanipulation – the positioning and precise movement of micron-sized objects.

	Radius (m)	**Surface/volume (m^{-1})**
Atom	10^{-10}	3×10^{10}
Grain of sand	2×10^{-4}	15×10^{3}
Table-tennis ball	0.02	150
Soccer ball	0.1	30

Table 2.3. *Some values of the surface/volume ratio*

gripper. For a detailed analysis (and calculations) of the pick and place, see [HALI 02] and [ROL 00].

Depending on the nature of the object to be moved, it is also possible to choose two surfaces made of materials A and B and a gripper made of material C in order to move the object from A to B without having to tilt the gripper by an angle θ. Careful selection of the three materials can ensure that the gripper–object adhesive force is greater than that between material A and the object, but less than the adhesion between material B and the object.

In order for the manipulation described above to be successful, the following double inequality between Hamaker's constants need to be satisfied [ROL 00]:

$$A_{(\text{object–material B})} > A_{(\text{gripper–object})} > A_{(\text{object–material A})} \quad [2.37]$$

2.5.3. *Nanofriction*

Figure 2.31 shows the variation of the friction force as a function of the normal load for a silicon tip (of a few nanometers of radius of curvature) covered with an amorphous layer of carbon, sliding on the surface of mica or carbon samples.

Because of surface forces, we note the existence of non-zero friction even with no applied load ($Ft^* = 0$ to 15 nN depending on the radius of curvature of the tip and the nature of the samples tested) [PIE 99, SCH 97a, SCH 97b]. The friction force cancels for a negative applied normal force P^* (maximum adhesive force) between 2 and 50 nN.

This result illustrates the complex nature of nanotribology compared to classical tribology, and shows that problems linked to friction and wear in microsystems cannot be resolved through the naive transposition of laws and empirical solutions that are valid on the macroscopic scale. Indeed, the size factor (the scaling from macro to micro, or even nano) is not beneficial to miniaturization because, in microsystems, the forces dissipated by friction in mechanical links are considerable [MIN 98].

Under these conditions, the material degradation mechanisms involve mechanical processes (such as abrasion, yield and fracture) as well as chemical processes (such as passivating, dissolution and oxidation). The combination of these mechanical and chemical (or *chemo-mechanical*) effects can lead to the catastrophic acceleration of material degradation via extensive material loss. Indeed, the effect of synergy between mechanical wear and chemical corrosion results in a total volume of removed material (Vt) which can in fact exceed the sum of material separately removed through wear and corrosion.

The volume Vt is given as a function of three components:

$$Vt = Vw + Vc + Vs \qquad [2.45]$$

where Vw and Vc are the volume of material removed separately by the effects of wear and corrosion, respectively, and Vs represents the synergistic effect between wear and corrosion which can account for 20–70% of the total volume of material removed [GROG 92, MIY 90, MOON 91, ZHANGT 94].

2.8.1. *Tribocorrosion*

Tribocorrosion phenomena are observed in a large number of applications and in many different environments. Some typical examples of such occurrences include:

– in the moving parts of an engine such as pistons, cylinders and valves with lubricants;

– with eyeglass frames, due to friction with the skin in the presence of perspiration;

– with electrical connectors (when there is insertion and removal in a humid or corrosive environment);

– with joint prostheses (when friction occurs in a physiological liquid);

– with components used in plumbing and pump technology.

Tribocorrosion is also an important aspect of chemo-mechanical polishing (CMP) processes that affect the manufacturing of parts for micromechanics as well as silicon wafers for microelectronics and nanotechnology.

Erosion-corrosion occurs in pipelines used to transport corrosive liquids mixed with abrasive particles, such as an acid containing ceramic particles or seawater or petrol containing sand. These examples mainly concern the chemical and petrochemical industries, but erosion-corrosion attacks the majority of mechanisms operating in environments where sand is present in significant quantities.

Tribocorrosion studies are carried out through the use of specific set-ups comprising an electrochemical cell and a tribometer, allowing the sample to be subjected to friction under either a free or an applied electrochemical potential. The main quantities measured are the coefficient of friction and the corrosion current.

Figure 2.40 shows the principle of an experimental set-up designed for the study of tribocorrosion. When the sample is polarized, its behavior under friction is significantly modified.

Many studies have shown the strong influence of the electrochemical potential of a surface on its tribological behavior [MIS 93, TAK 96, YON 06].

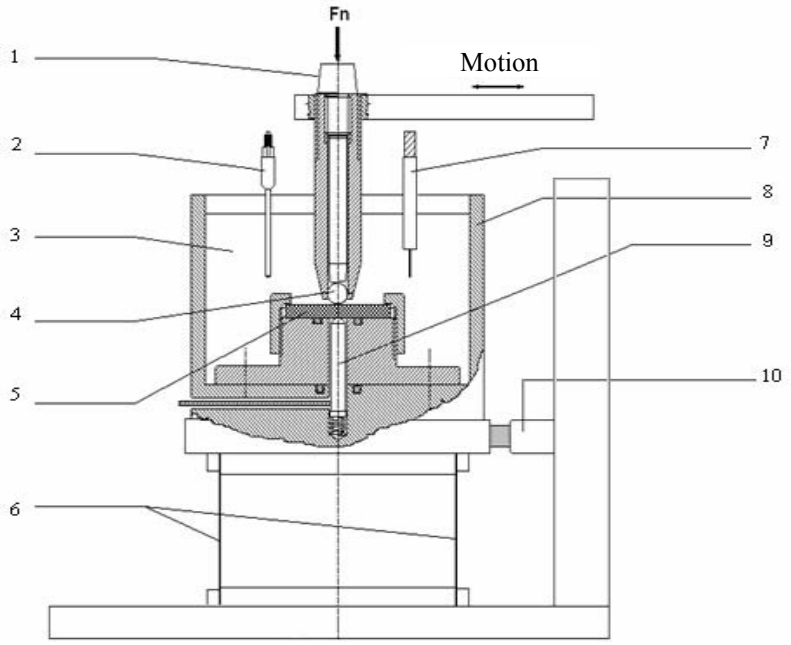

Figure 2.40. *Tribocorrosion analysis set-up: 1) normal applied load; 2) reference electrode; 3) electrolyte; 4) ceramic sphere; 5) sample; 6) spring plates; 7) platinum counter-electrode; 8) PTFE electrochemical cell; 9) towards the potentiostat; 10) force sensor (adapted from [TAK 96])*

The tribocorrosion of nickel and iron in a sulfuric environment (H_2SO_4 1N) is the focus of a previous study [TAK 96]. The electrochemical behavior of nickel in this environment is illustrated by the polarization curve as seen in Figure 2.41.

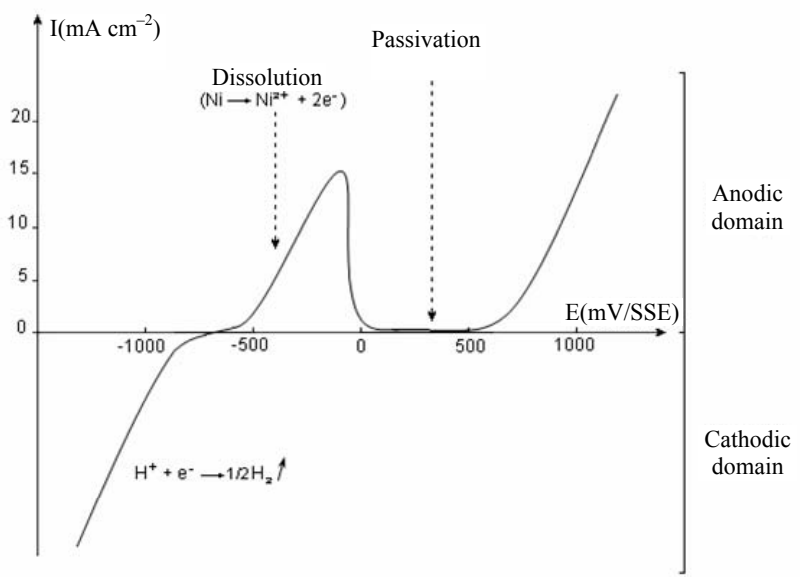

Figure 2.41. *Polarization curve (intensity-contact potential) of nickel in a sulfuric environment (H_2SO_4 1N); contact potentials are given relative to a saturated sulfate reference electrode (SSE)*

In the anodic domain, the curve shows a dissolution peak followed by a passivation plateau that corresponds to the formation of a film made up of a nickel oxide and nickel hydroxide mixture.

Several friction tests were performed on the material using an aluminum sphere of 5 mm in diameter and a normal load of 3.5 N. A number of different polarization potentials were used, corresponding to the cathodic domain (–1300 mV/SSE), the dissolution domain (–300 mV/SSE), the corrosion potential (–650 mV/SSE) and the passivation plateau (500 mV/SSE).

For the samples subjected to the corrosion potential or placed in the cathodic domain, we note only slight surface wear (see Figure 2.42c). The sample in the dissolution domain suffers significant losses of material due to the combined effects of corrosion and friction wear (see Figure 2.42a). Indeed, the synergy between

electrochemical corrosion and wear leads to a proportional rate of material loss which increases as a function of the polarization potential and can represent up to 40% of the total loss of material (see Figure 2.43). Figure 2.42b shows that no wear appears on the surface of the sample polarized to 500 mV/SSE in the passivation domain, and we conclude that the passivation film provides excellent protection to the material.

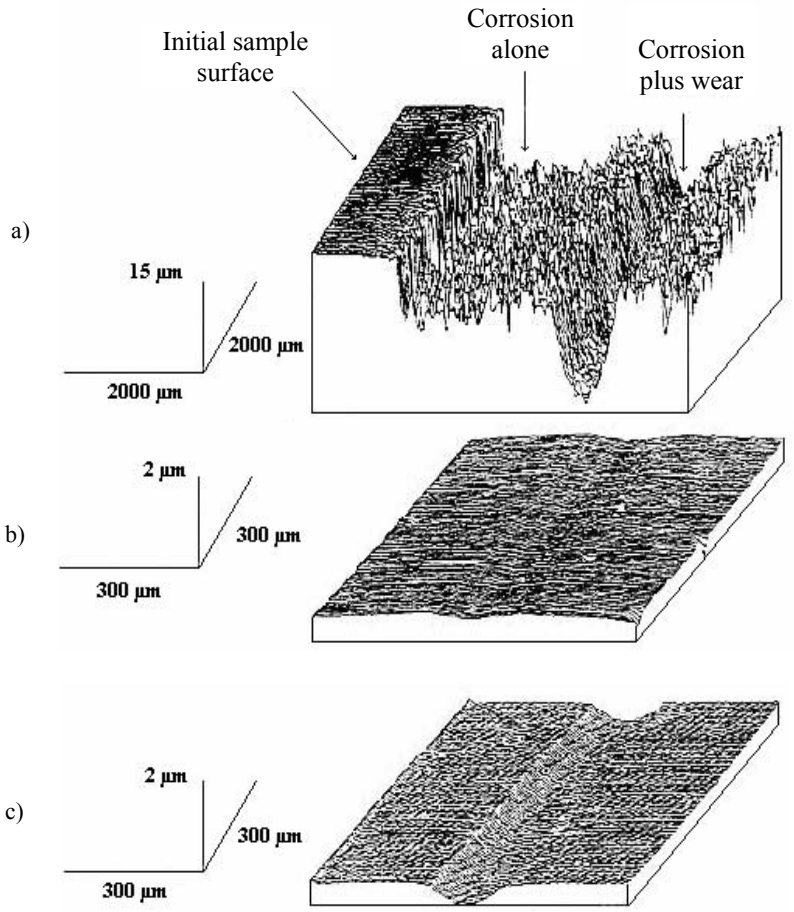

Figure 2.42. *Surface states of nickel samples following a friction test in a H_2SO_4 1N medium. The sample potential is: a) –350 mV, b) 500 mV, c) –650 mV (equally at –1300 mV). The reference surface (Figure 2.42a) is the initial sample surface protected during the tribocorrosion test [TAK 97c]. Potentials were measured relative to a saturated sulfate electrode*

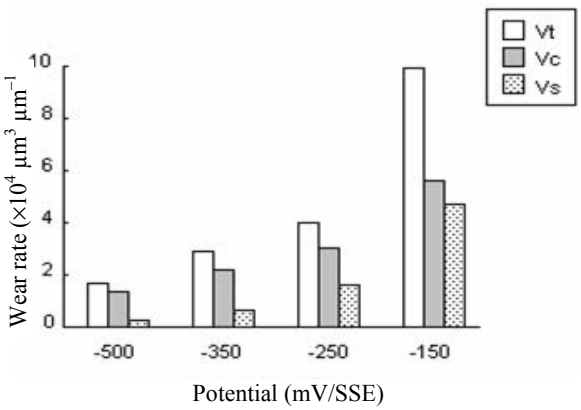

Figure 2.43. *Volumes of material removed by tribocorrosion as a function of the applied potential imposed on nickel. Vw, Vc, Vs and Vt are the volumes defined in the text (see equation [2.45]). When measured in the cathodic domain, volume Vw (–1300 mV) is 130 µm³ µm⁻¹) [TAK 97c]*

Other materials have a similar behavior to nickel. This is the case for iron when it is in a high concentration acidic medium (H_2SO_4 > 10 M) [MIS 93], and for copper [YON 06] or brass [QIU 02] when placed in a sodium laurylsulfonate medium with the addition of 0.1 M sodium sulfate.

For the case of brass in sliding contact against a silicon nitride sphere, Figure 2.44 shows the evolution of the friction coefficient as a function of the applied potential. When the potential is close to or greater than the corrosion potential (–0.444 V) measured relative to a saturated calomel electrode (SCE), a passivation film forms on the surface of the material. This acts as a lubricant and significantly reduces the friction coefficient as well as the surface wear (the measured friction coefficient is 0.07). Conversely, when the material is brought into the cathodic domain, the protective oxide film disappears due to hydrogen evolution which cleanses the surface and makes it more active. This yields a higher friction coefficient and a lower resistance to wear (the measured friction coefficient is 0.27).

However, note that the passivation film does not necessarily always grant the material good protection against wear. Indeed, the opposite is sometimes observed [BIE 00]. In this work, the authors studied the behavior under friction of tungsten against an aluminum sphere in media 0.5 M H_2SO_4 and 0.1 M $K_3Fe(CN)_6$ at pH 3. The applied load was 5 N and the sliding speed 62 mm s^{-1}.

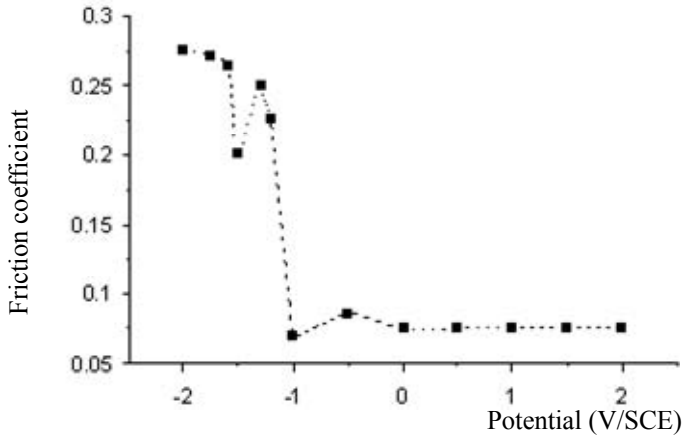

Figure 2.44. *Variation of the friction coefficient of brass against a SiO_2 sphere under a load of 9.8 N in a sodium laurylsulfonate solution with 0.1 M sodium sulfate. Values for the friction coefficient were recorded under several applied potentials [QIU 02]*

Figure 2.45 shows the wear volumes measured under different applied potentials. In an H_2SO_4 medium and under a cathodic potential, the detected wear is negligible. When no potential is imposed (i.e. with a corrosion potential of 60 mV), some material wear is measured as shown in Figure 2.45a. When a potential corresponding to the passivation of the surface (formation of tungsten oxide) is applied (380 mV relative to an Ag/AgCl electrode), a significant increase in wear is observed (see Figure 2.45b).

An additional test, carried out in a highly oxidizing medium ($K_3Fe(CN)_6$) with a corrosion potential of 380 mV relative to an Ag/AgCl electrode, recorded significant wear comparable to that obtained in a H_2SO_4 medium polarized in the anodic domain.

These results clearly show that oxidation of a surface contributes to its wear. The oxide degrades under friction and exposes the naked surface of the material which in turn oxidizes again when in contact with the electrolyte.

Similar results have been obtained for TiN coatings deposited on a steel substrate and subject to friction against an aluminum sphere in a borate medium (0.3 M H_3BO_3 and 0.075 M $Na_2B_4O_7$). When the material is polarized in the anodic domain, the oxidation of TiN and the generation of TiO_2 accelerate the surface wear under friction [BAR 01]. This is essentially due to the mechanical properties of TiO_2 which are much weaker than those of the TiN compound.

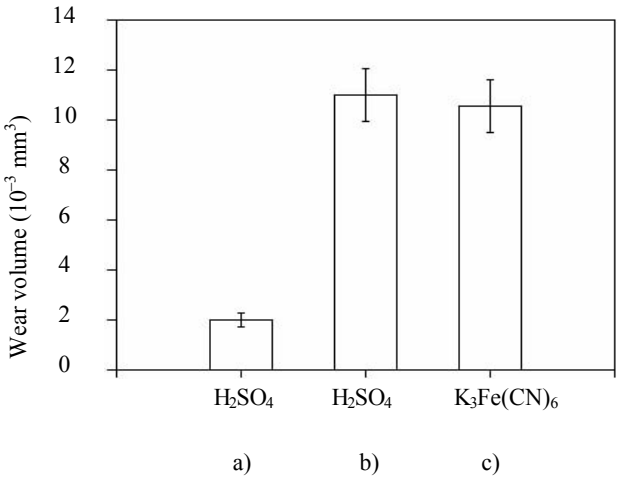

Figure 2.45. *Influence of the imposed electrochemical potential on tungsten wear: a) in H_2SO_4 0.5 M (under free potential E = 60 mV); b) in H_2SO_4 0.5 M (under imposed potential E = 380 mV); c) in $K_3Fe(CN)_6$ (under free potential E = 380 mV). The potentials are given relative to an Ag/AgCl electrode. Friction was imposed with an aluminum sphere of 5 mm in diameter sliding alternatively at a speed of 62 mm s^{-1} [BIE 00]*

In another publication [MIS 99], the authors studied the behavior of 34CrNiMo6 steel under friction against an aluminum sphere in a basic medium. They showed that anodic polarization (or passivation) of the material led to the generation of a surface oxide film that rapidly degrades under friction, whereas the same material showed improved resistance to wear in the cathodic phase. The wear mechanism reported by the authors consists of the growth of a weakly adhesive oxide film that deteriorates under friction, then eliminated as wear debris. The repetition of this mechanism of generation and degradation of the oxide film leads to the progressive consumption of the material and increasingly severe wear.

As a rule, the composition, stability and protective performance of steel passivation films depend on their composition, the type of electrolyte and the imposed potential.

Contrary to 34CrNiMo6 steel, with a passivation film which degrades easily under friction, stainless steels generate more stable surface passivation films which grant the materials better wear resistance [JIA 93, TAK 97c]. However, under particularly severe conditions (greater sliding speed and/or load), the passivation film can be destroyed and the material dissolved [PON 04].

3.2.4.1. *Friction and wear of ceramics*

In order to understand the mechanisms of crack propagation and wear in ceramics, we consider the case of sliding contact between a sphere of radius R and a ceramic plane. If C is the length of a crack in the contact area and F the normal load applied to the sphere, it can be shown that crack propagation occurs when the normal applied load reaches the critical value F_c [ZUM 96]:

$$F_c = 1.1\frac{\pi^{7/2}}{(1-2\nu)^3}\frac{K_C^3 R^{4/3}}{(1+C^*\mu)^3 C^{3/2} F^{2/3} E^{4/3}} \quad [3.1]$$

where

$$C^* = \frac{3\pi}{8}\frac{4+\nu}{1-2\nu} \quad [3.2]$$

and ν and E are Poisson's coefficient and Young's modulus, respectively, μ is the friction coefficient between the sphere and plane and K_c is the fracture toughness of the ceramic.

By introducing two new terms (H and β, the hardness and the ratio of apparent and real contact area, respectively), equation [3.2] becomes:

$$F_c = \frac{2\pi}{1.12\beta(1-2\nu)}\frac{K_C RH}{(1+C^*\mu)C^{1/2}F^{1/2}\ E^{1/2}} \quad [3.3]$$

When the applied load is equal to or greater than the critical value F_c, crack propagation occurs, which is generally followed by grain pull-out and rapid wear of the surface (see Figure 3.7).

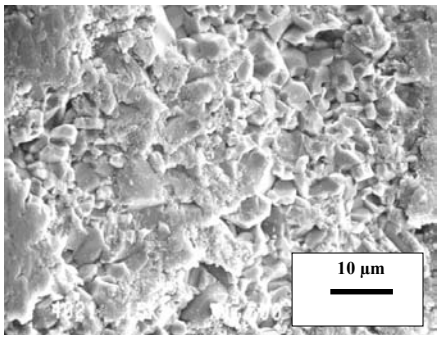

Figure 3.7. *Alumina surface showing significant wear of the material characterized by grain pull-out*

The mechanical surface characteristics of ceramics can also be significantly improved by treatments such as ion implantation or laser surface melting [POS 05, ZUM 00]. Laser surface melting involves depositing a layer of a given material onto the surface of a ceramic before irradiation by a high-energy laser beam, capable of melting it to form a new alloy or to precipitate new phases over a depth of a few hundred microns. Thus, starting from a suspension of powdered ceramics, HFO_2, TiN and ZrO_2 films have been deposited onto the surface of alumina samples with the addition of tungsten powder. After drying, these layers were heated to 1,500°C before being irradiated with a CO_2 laser beam. Friction tests carried out with an alumina sphere showed that the performed surface treatment resulted in a reduction in the wear by a factor of 4–8 and a reduction in the friction coefficient by a factor of 2 [ZUM 00].

As a general rule, the tribological behavior of ceramics is susceptible to humidity which can impact in two ways:

– the acceleration of crack propagation and, consequently, of material wear (in this case, the underlying physical mechanism is the breaking of inter-atomic bonds following their interaction with water molecules); and

– the tribochemical formation of a film (generally oxide/hydroxide) that is able to lubricate the contact and protect the surface.

Depending on the nature of the ceramic, the applied stress conditions and the level of humidity, these two phenomena can either occur simultaneously and compete, or occur independently. This potentially complex interaction accounts for the often contradictory results found in work published on the tribological behavior of oxide ceramics such as alumina and zirconia [CHENY 91, FIS 98, LAN 90, TAK 93b, TAK 93c].

For non-oxide ceramics, and more specifically silicon nitride and silicon carbide, all results point to a systematic reduction of the friction coefficient when the level of residual humidity increases.

The tribological behavior of these ceramics in the presence of humidity is governed by the following tribochemical reactions:

$$Si_3N_4 + 6H_2O \rightarrow 3\ SiO_2 + 4NH_3 \quad [3.4]$$

$$SiC + O_2 + H_2O \rightarrow SiO_2 + CO + H_2 \quad [3.5]$$

$$SiO_2 + 2H_2O \rightarrow Si(OH)_4 \quad [3.6]$$

These reactions lead to the formation of a film consisting of a silicon oxide/hydroxide compound, which protects the surface and acts as a lubricant [LAN 90, TAK 94a, TAK 94b].

Figures 3.8 and 3.9 show the results of friction tests illustrating the beneficial effect of humidity on friction and on the wear of the Al_2O_3/Al_2O_3 and SiC/SiC pairs [TAK 94b]. The results of the tests presented in these figures characterize friction between a ceramic sphere of 5 mm in diameter and a plane sample at residual humidity levels of 20, 50 and 90%.

The figures show that in dry conditions or with low humidity, friction and wear are both significant. Moreover, when the applied load is increased, the level of wear occurring in the material becomes catastrophic [GAV 02b] in accordance with equation [3.3]. Indeed, this equation clearly shows that any increase in the normal applied load or friction coefficient brings about a reduction in the critical fracture load F_c, thus accelerating material wear.

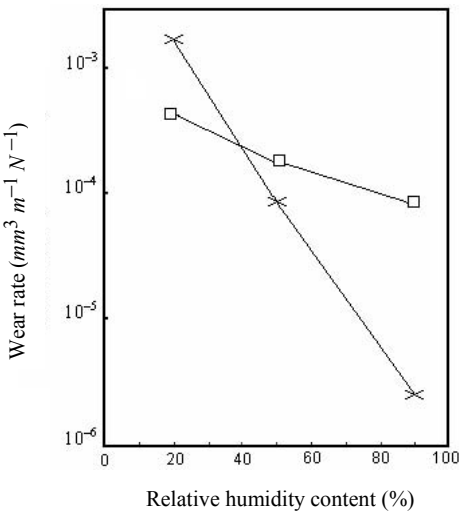

Figure 3.8. *Variations in the rate of wear of Al_2O_3/Al_2O_3 (□) and Si/SiC(×) couples/ pairs as a function of residual humidity. Tests were carried out with a reciprocating tribometer operating in the sphere/plane set-up and using a 5 mm diameter sphere under a normal applied load of 30 N. The sliding distance is 2 cm and the sliding speed is 2 mm s^{-1} [TAK 94b]*

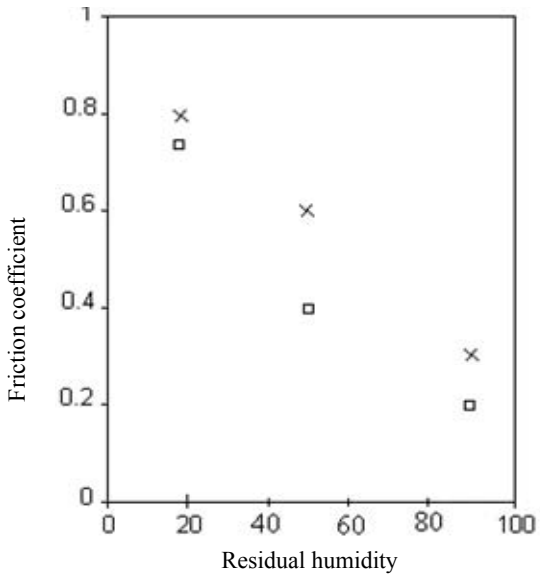

Figure 3.9. *Variations of the friction coefficient as a function of residual humidity: Al_2O_3/Al_2O_3 (×) and SiC/SiC (□) pairs (see Figure 3.8 for a description of the tests)*

Table 3.4 summarizes the data available in the literature in order to provide a qualitative overview of the influence of the applied load-humidity pair on the tribological behavior of ceramic materials when a protective and lubricating oxide/hydroxide film forms in humid conditions.

	Light load	**Moderate load**	**Heavy load**
Low humidity level (< 30%)	Moderate wear (10^{-4} – 10^{-6})	Severe wear (10^{-3} – 10^{-4})	Extensive wear (> 10^{-3})
Moderate humidity level (30–70%)	Low wear (10^{-6} – 10^{-8})	Transitional zone (low to severe wear)	Severe wear (10^{-3} – 10^{-4})
High humidity level (> 70%)	Very low wear (< 10^{-8})	Low wear (10^{-6} – 10^{-8})	Moderate wear (10^{-4} – 10^{-6})

Table 3.4. *Qualitative overview of the extent of ceramic wear as a function of the residual humidity and contact pressure for ceramic/ceramic pairs. Order-of-magnitude values for residual humidity (RH) as well as rate of wear (given in* $mm^3\ m^{-1}\ N^{-1}$*) are given in brackets. The notions of light, moderate or heavy load are defined relative to* F_c *(equation [3.3]). The data presented only applies to ceramics which become coated with a protective, lubricating oxide/hydroxide film under humid conditions*

We also note that ceramics are sintered materials and therefore have varying degrees of porosity, impurities, agglomerates and vitreous phases at grain boundaries. These structural or chemical defects are precisely the sites from where cracks can develop before propagating between and within the ceramic grains. Materials manufactured under different sintering conditions and from ceramic powders of varying purity generally exhibit different tribological behavior. This partly explains certain results which can at times seem contradictory. The significant role played by these inter-granular vitreous phases needs to be stressed: indeed, at high temperatures (typically above 800°C), these secondary phases become viscous and radically alter the mechanical properties and tribological behavior of the ceramic material.

Concerning metal-ceramic couples, numerous studies have shown that the chemical reactivity of the metal is a determining factor in the tribological behavior of the pair under friction [BUC 81, BUC 94, PEP 76, TAK 92, TAK 93a].

Ultra-vacuum studies of friction between alumina and various metals (Ag, Cu, Ni and Fe, chosen as a function of their oxide stability which increases from Ag to Fe) were carried out and allowed us to establish that the adhesive contact between opposing surfaces could be perfectly correlated to the free energy of formation of the

metallic oxides. This finding is in perfect agreement with the hypothesis that interfacial adhesion occurs *via* the generation of genuine chemical bonds between the metallic cation and the oxygen anion of alumina. When the metallic surfaces are exposed to oxygen, dioxides and trioxides such as $CuAlO_2$ or $NiAl_2O_3$ form at the interface during friction, resulting in an increase of the metal-ceramic adhesion and a subsequent increase of the friction coefficient [PEP 76].

In the case of transition metals, many authors have reported a strong correlation between the filling of the valence band (d-state) and the metal's reactivity. The surface is less reactive as the valence band is increasingly filled, leading to lower measured friction coefficients between the metals and various ceramics [BUC 94, MIY 82].

3.2.5. *Cermets*

A cermet is a composite composed of ceramic and metallic materials. Cermets possess both hardness and ductility as they combine a hard phase (the ceramics) and a soft phase (the metallic binding). When a crack forms within the ceramic, its propagation to adjacent grains is arrested by contact with the more ductile metallic phase (see Figure 3.10).

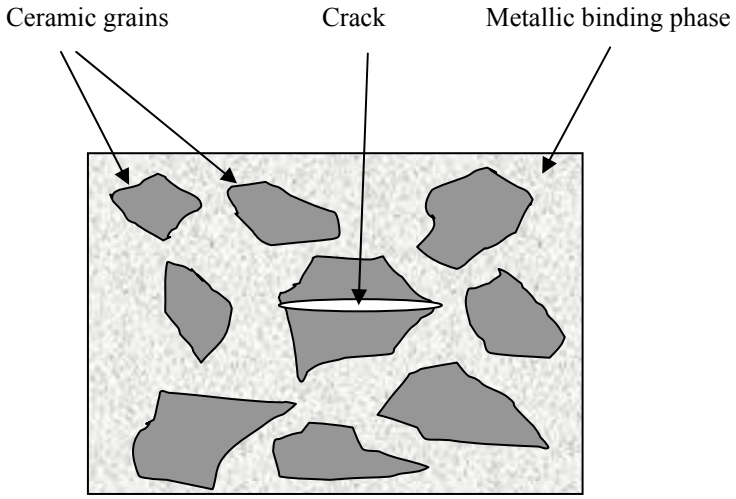

Figure 3.10. *Crack propagation through the ceramic grain is stopped by the metallic phase*

Cermets can be divided into two classes: tungsten-carbide (WC)-based cermets and other carbide-based cermets.

3.2.5.1. *Tungsten-carbide (WC)-based cermets*

These materials are produced from WC powders mixed into a cobalt binding agent, subsequently sintered at a temperature of about 1,500°C. At this temperature, the cobalt powder melts and the molten metal fills in the voids and thus binds the carbide grains together (see Figure 3.10).

The percentage of cobalt used is 5–20% by weight and the WC grains are generally 1–10 µm in diameter. The use of nanograins with diameters in the range of 0.1–1 µm makes it possible to generate materials presenting elevated hardness and improved wear resistance.

When the WC-Co carbide is subjected to friction, we initially see preferential wear of the binding phase (Co) followed by cracking and the subsequent loosening of the carbide grains [PIR 06, SHI 05].

The hardness and wear of the material strongly depend on the concentration of the binding phase. This is clearly shown in Figure 3.11 where we see an increase in wear and a decrease in hardness as a function of cobalt concentration. In contrast to the hardness, the fracture toughness increases with cobalt concentration from 8 to 14 MPa $m^{1/2}$ as the percentage of cobalt increases from 3 to 14% [PAST 87].

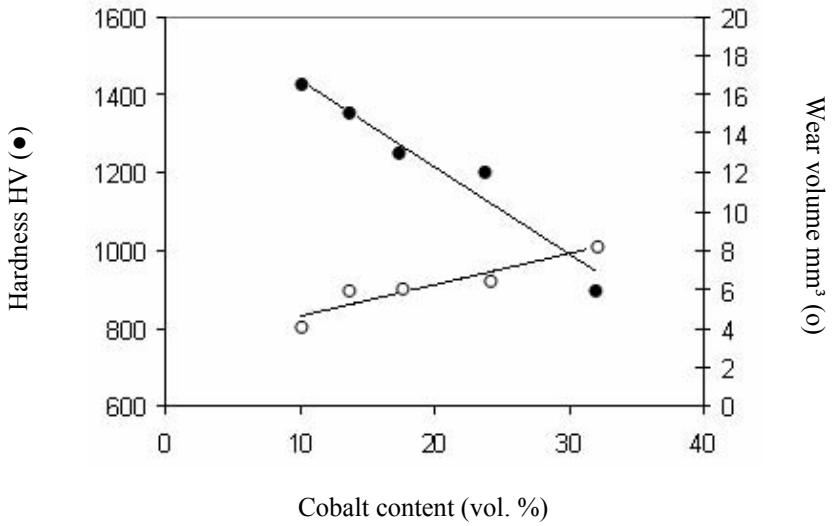

Figure 3.11. *Variation of the hardness and volume wear of the WC-Co cermet as a function of the binding phase concentration. The tribometer used is of the pin-on-cylinder type and the applied load is 40 N [PAST 87]*

Finally, we note that the wear resistance of tungsten carbide is improved through the addition of other carbides such as TiC, TaC and NbC or through the use of mixed carbides such as (W,Mo)C, (W,Ti)C or WC-(W,Ti)C-TaC.

3.2.5.2. *Other carbide-based cermets*

Examples of such composites may include TiCN-Ni, TiC-Ni, WC-TiN-TiC-Co, (Ti,Mo)CN-Ni, TiC-NiMo or TiCN-WC-Ni.

These materials are generally harder than WC-based cemented carbides and their resistance to wear is greater. When applied to cutting tools, they can significantly extend their lifespan and provide improved cutting quality [CEL 06, NIN 05, WAL 06].

As well as their application to cutting tools (for wood, metal or ceramics), cermets are also widely used as coatings on drilling heads, as well as hammering and shaping tools used in stamping, embossing and forging.

3.3. Surface treatments and coatings [BHU 91, CART 00]

There are many different techniques for surface treatments and coatings: they differ in their basic principles, their ease of practical implementation and the precise way in which they modify the surface of the treated materials.

Depending on the target application and its particular requirements, we can select techniques to modify the hardness, surface energy, friction coefficient, residual stresses, appearance or indeed any other mechanical, physico-chemical or aesthetic property of the surface.

Surface treatment and coating techniques can be classified into two categories:

– conversion techniques which modify the composition and/or structure of the surface to be treated; and

– deposition techniques which coat the surface to be treated with a thin layer of a given material.